REPORT DOCUMENTATION PAGE

Form Approved
OMB No. 0704-0188

1. AGENCY USE ONLY (Leave blank)	2. REPORT DATE	3. REPORT TYPE AND DATES COVERED
	September 1996	Final - Oct 93 - May 95

4. TITLE AND SUBTITLE
Retinal Damage and Laser-Induced Breakdown Produced by Ultrashort-Pulse Lasers

5. FUNDING NUMBERS
C - F33615-92-C-0017
PE - 62202F
PR - 2312
TA - A1
WU - 01

6. AUTHOR(S)
Clarence P. Cain, Cher 1 D. DiCarlo, Benjamin A. Rockwell, Paul K. Kennedy, W.P. Roach, Gary D. Noojin, David J. Stolarski, Daniel X. Hammer, and Cynthia A. Toth

7. PERFORMING ORGANIZATION NAME(S) AND ADDRESS(ES)
TASC, Incorporated
750 East Mulberry
Suite 302
San Antonio, TX 78212-3159

8. PERFORMING ORGANIZATION REPORT NUMBER

9. SPONSORING/MONITORING AGENCY NAME(S) AND ADDRESS(ES)
Armstrong Laboratory
Occupational and Environmental Health Directorate
8111 18th Street
Brooks Air Force Base, TX 78235-5215

10. SPONSORING/MONITORING AGENCY REPORT NUMBER
AL/OE-JA-1995-0079

11. SUPPLEMENTARY NOTES

12a. DISTRIBUTION/AVAILABILITY STATEMENT
Approved for public release; distribution is unlimited.

12b. DISTRIBUTION CODE

13. ABSTRACT *(Maximum 200 words)*

In vivo retinal injury studies using ultrashort-pulse lasers at visible wavelengths for both rabbit and primate eyes have been completed, and the results are presented herein for laser-induced breakdown (LIB) and bubble generation. Results of previous measurements for the minimum visible lesion (MVL) threshold doses for both primate and rabbit eyes were reported earlier for pulsewidths from 4 nanoseconds (ns) to as low as 90 femtoseconds (fs). We have recorded on video the first *in vivo* LIB in vitreous using both albino (New Zealand white) and pigmented (Dutch-belted) rabbit and rhesus monkey eyes with 580-nanometer (nm), 120-fs pulses. We believe the phenomena responsible for bubble generation to be LIB because of the extremely high irradiances within the focused beam and because of the very low absorption properties of the vitreous humor. The laser-generated LIB-ED_{50} bubble threshold for the monkey eye was 0.56 μJ at 120 fs. Results of our nonlinear modeling and calculations for self-focusing within the eye and for LIB thresholds are presented and are compared with our experimental results. Data is presented which show that LIB thresholds cannot be reached with MVL-ED_{50} doses until the pulsewidth drops to <600 fs and the retinal image diameter is close to 10 micrometers (μm). Self-focusing and LIB are the two nonlinear effects shown to affect the visible lesion thresholds, and our results also explain why it is so difficult to produce hemorrhagic lesions in either the rabbit or primate eye with visible 100-μJ, 100-fs laser pulses.

14. SUBJECT TERMS	15. NUMBER OF PAGES
Bubble generation; LIB; MVL thresholds; Retinal injury; Self-focusing; Ultrashort-pulse lasers; Visible lesions; Vitreous humor	10
	16. PRICE CODE

17. SECURITY CLASSIFICATION OF REPORT	18. SECURITY CLASSIFICATION OF THIS PAGE	19. SECURITY CLASSIFICATION OF ABSTRACT	20. LIMITATION OF ABSTRACT
Unclassified	Unclassified	Unclassified	UL

Graefe's Arch Clin Exp Ophthalmol (1996)
234: S 28–S 37 © Springer-Verlag 1996

Clarence P. Cain
Cheryl D. DiCarlo
Benjamin A. Rockwell
Paul K. Kennedy
Gary D. Noojin
David J. Stolarski
Daniel X. Hammer
Cynthia A. Toth
W. P. Roach

Retinal damage and laser-induced breakdown produced by ultrashort-pulse lasers

Received: 21 July 1995
Revised version received:
13 October 1995
Accepted: 13 November 1995

C.P. Cain (✉) · G.D. Noojin
D.J. Stolarski
TASC, 750 East Mulberry, Suite 302,
San Antonio, TX 78212–3159, USA
Tel. +1-210-536 3709;
Fax +1-210-534 0420

C.D. DiCarlo
Uniformed Services University of the
Health Sciences, 4301 Jones Bridge
Road, Lab Animal Medicine Department,
Bethesda, MD 20814–4799, USA

B.A. Rockwell · P.K. Kennedy
D.X. Hammer
Armstrong Laboratory, Optical Radiation
Division, 8111 18th Street, Brooks AFB,
TX 78235-5215, USA

C.A. Toth
Duke University Eye Center, Box 3802,
Durham, NC 27710, USA

W.P. Roach
Air Force Office of Scientific Research,
Directorate of Chemistry and Life
Science, 110 Duncan Avenue, Suite B115,
Bolling AFB, DC 20332, USA

Abstract ● Background: In vivo retinal injury studies using ultrashort-pulse lasers at visible wavelengths for both rabbit and primate eyes have shown that the degree of injury to the retina is not proportional to the pulse energy, especially at suprathreshold levels. In this paper we present results of calculations and measurements for laser-induced breakdown (LIB), bubble generation, and self-focusing within the eye. ● Methods: We recorded on video and measured the first in vivo LIB and bubble generation thresholds within the vitreous in rabbit and primate eyes, using external optics and femtosecond pulses. These thresholds were then compared with calculations from our LIB model, and calculations were made for self-focusing effects within the vitreous for the high peak power pulses. ● Results: Results of our nonlinear modeling and calculations for self-focusing and LIB within the eye were compared with experimental results. The LIB ED_{50} bubble threshold for the monkey eye was measured and found to be 0.56 μJ at 120 fs, compared with the minimum visible lesion (MVL) threshold of 0.43 μJ at 90 fs. Self-focusing effects were found to be possible for pulsewidths below 1 ps and are probably a contributing factor in femtosecond-pulse LIB in the eye. ● Conclusions: Based on our measurements for the MVL thresholds and LIB bubble generation thresholds in the monkey eye, we conclude that in the femtosecond pulsewidth regime for visible laser pulses, LIB and self-focusing are contributing factors in the lesion thresholds measured. Our results may also explain why it is so difficult to produce hemorrhagic lesions in either the rabbit or primate eye with visible 100-fs laser pulses even at 100 μJ of energy.

Introduction

Retinal injury studies using laser pulses have been performed since the advent of pulsed laser systems because lasers can damage the retina in a single pulse. These studies were performed to determine the hazards for laser pulses from the millisecond time scale to the femtosecond time scale. The endpoint in most of these studies has been an ophthalmoscopically determined minimum visible lesion on the retina and, as a secondary requirement, an observable lesion through fluorescein angiography. Histopathology has also been performed on many of the lesions created by the intense pulses to determine the damage mechanisms or at least the type of cellular damage done to the retinal cells, pigmented epithelium, and/or choroid. A large data bank exists for retinal damage done by laser pulses of microsecond and nanosecond durations, but less information exists for picosecond and femtosecond pulses. Until recently, there has not been enough published information to support laser safety standards such as the ANSI or IEC standards for picosec-

ond and femtosecond laser pulses, although these laser systems are proliferating. Recent studies [2, 5, 6, 8, 13, 14, 21, 25, 35–37, 42] provide data for MVL-ED_{50} thresholds in both rabbit and rhesus monkey eyes for picosecond (3–30 ps) and femtosecond (80–600 fs) pulses. The data do not always agree, and some of the results suggest different damage mechanisms at the shortest pulses generated. For instance, it has been found that fluorescein angiography is a more sensitive indicator of retinal damage in the pigmented rabbit eye than the ophthalmoscopic MVL (minimum visible lesion) endpoint for ultrashort pulses [2, 36]. However, the reverse is true for the rhesus monkey eye [8], which presents small retinal image diameters when compared with the rabbit. This difference could possibly be accounted for by the difference in species (i.e., focusing properties of the eye, fundus pigmentation, fovea, etc.).

Another reported phenomenon that raises questions is the ability of the eye to withstand about 100-fs laser pulses with energies of 100 times the MVL-ED_{50} thresholds without suffering hemorrhagic lesions or catastrophic damage to the retina. Damage to the retina does not appear to be proportional to the energy delivered to the eye, and this characteristic has been seen in both rabbit and monkey eyes [6, 8, 36, 37, 42]. With these very large pulse energies (about 100 μJ) the size of the lesion increases somewhat, but not in proportion to the energy increase. Choroidal hemorrhagic lesions can be produced with these high-energy pulses, but not at the rate or at energy levels one would expect. Intraretinal hemorrhages (rupture of blood vessels visible within the retina) can easily be produced with 90-fs pulses [8] at energies as low as 0.83 μJ (580 nm). Thus, there appears to be a major difference between hemorrhages produced within the retinal vessels and those produced within the choriocapillaris. It appears as if some mechanism (possibly nonlinear) within the eye limits the amount of energy reaching the retinal pigmented epithelium and choroid at these 80- or 90-fs pulsewidths, in contrast to nanosecond pulses [3, 41].

One other phenomenon reported with ultrashort-pulse threshold data is a variation in the time required for MVLs to develop as the pulsewidth becomes shorter [8, 42]. For nanosecond and picosecond pulsewidth data, visible lesions appear almost immediately or within the first 10 min after exposure. However, as the pulsewidth decreases to the femtosecond regime, it takes longer for the lesions to appear. In fact, for 90-fs pulses, the number of lesions developing between 1-h and 24-h postexposure can increase by a factor of one and a half. Thus, there appears to be some inverse relationship between laser pulsewidth and the time required for lesions to develop. This may be connected to a change in the damage mechanism for shorter pulsewidths.

Because our MVL thresholds in the picosecond and femtosecond regimes were lower than the nanosecond and microsecond laser pulse thresholds reported by others, we examined how nonlinear optical phenomenon can affect the characteristics of light propagating through the eye and, hence, change the minimum energy required to produce retinal damage. Nonlinear optical phenomena that occur in optically homogeneous materials like ocular media include self-focusing, stimulated Brillouin scattering, supercontinuum generation, laser-induced breakdown (LIB), and nonlinear absorption. After examining all the relevant thresholds, we have determined that self-focusing and LIB are the phenomena most likely to affect our measured thresholds [16, 28].

The approach used to investigate these problems included theoretical modeling of the systems and mechanisms with linear and nonlinear parameters for the component parts of the eye. Models were developed to predict the effects of self-focusing [27] within the eye and to calculate LIB thresholds [19]. The results from these models were compared with our experimental results for MVL thresholds. In addition to the modeling, experimental measurements were made for the ocular component properties, such as the nonlinear component of the index of refraction [26], n_2, LIB thresholds [7, 9], artificial eye retinal image diameters, and plasma spectroscopy [34].

In this paper we present the results of our modeling and experimental efforts to elucidate the mechanisms contributing to and/or causing the unexpected results mentioned above. One concern we have had with our MVL-ED_{50} threshold data was that the slopes of the probit curves for the five pulsewidths were all above 2 with the exception of that for 90 fs, which was 1.58. While there is no established minimum for the slope, we expected it to be greater, as the others were all above 2. Thus we present data that can reasonably explain how the eye can withstand 100-μJ laser pulses at 90 fs, possible reasons for the delay in developing lesions, and why the slope of the probit curve at 90 fs is only 1.58 (considerably lower than the 4.11 at 600 fs).

Experimental methods

Experimental systems

For a complete description of the ultrashort-pulse laser system and measuring instrumentation, see Cain et al. [8]. An artificial eye was developed to simulate the optical properties of the monkey eye with a focal length of 12 mm, and it was filled with water or saline. A computer-controlled scanning knife edge was used to measure the focal image diameter within the water.

Bubble generation and video recording

In order to detect and record bubbles within the eye during exposure it was necessary to modify the Zeiss fundus camera to provide additional light intensity for the color video camera. As shown in Fig. 1, a high-intensity, fiberoptic light source was added to the

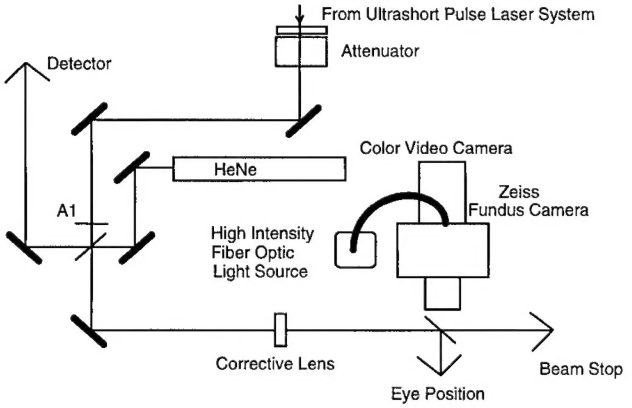

Fig. 1 Laser delivery system and video recording

camera and adjusted to illuminate the area of the retina being observed on the video camera and monitor. The intensity of the light irradiating the retina could be increased by an order of magnitude. Also shown in Fig. 1 is a He-Ne laser which could also be directed to the fundus for increased illumination. This He-Ne laser was used with the albino rabbit to record bubbles. It did not work satisfactorily with the pigmented rabbit eye or monkey eye; therefore, a fiberoptic light source was added. A corrective lens was placed before the beam-splitter at the eye; first to correct any refractive abnormalities of the eye, and second to move the focused image to be within the vitreous. The monkey eye required 1 D of corrective lens to focus the image at the retina. A 1-D lens was used to correct the refractive error, and it was placed 230 mm away from the eye to move the image 65 μm anterior to the retina. This lens placed the image within the vitreous for the LIB threshold measurements.

In vivo model

Rhesus monkeys from 2.2 to 6.9 kg in weight were maintained under standard laboratory conditions (12 h light, 12 h dark). Rhesus monkeys and rabbits (1.5–3.5 kg) were screened pre-exposure to determine how much correction was needed for their refractive errors. All procedures were performed during the light cycle. The treatment and procedures used in this study conformed to the Federal Guidelines for Use of Animals in Research and the research protocol USAFSAM Protocol RZV-91-04 [24].

In vivo preparation

Rhesus monkeys were chemically restrained using 10 mg/kg ketamine hydrochloride intramuscularly. Once each monkey had been restrained, 0.25 mg/kg atropine sulfate was administered subcutaneously. Two drops each of 0.5% proparacaine hydrochloride, 2.5% phenylephrine hydrochloride, and 1% tropicamide were administered to each eye. Under ketamine restraint, the monkey had intravenous catheters placed for administration of warmed lactated Ringer's solution (10 ml/kg per hour flow rate) and for administration of propofol. An initial induction dose of propofol (5 mg/kg) was administered to effect. The state of anesthesia was maintained using 0.2–0.5 mg/kg per hour of propofol via syringe pump. The monkey was intubated with a cuffed endotracheal tube. A peribulbar injection of 2% lidocaine with hyaluronidase was administered to reduce extraocular muscular movement. The monkey was securely restrained in a prone position on an adjustable stage for the laser exposure. The monkey's heart rate, blood pressure, and pulse were continuously monitored throughout the experimental protocol. The monkey's normal body temperature was maintained by the use of circulating warm-water blankets.

Rabbits were chemically restrained using 25 mg/kg ketamine HCl intramuscularly. A dose of 1–2 mg/kg atropine sulfate was administered subcutaneously. This high dose was administered to overcome the effect of atropinase enzyme in rabbits. Two drops each of 0.5% proparacaine hydrochloride, 2.5% phenylephrine hydrochloride, and 1% tropicamide were administered to each eye. Under ketamine restraint, the pinnae were clipped and surgically scrubbed and an intravenous catheter was placed in the marginal ear vein for administration of propofol. An initial induction dose of propofol (7.5–8.0 mg/kg) was administered to effect. The state of anesthesia was maintained in the rabbit using 0.7–0.8 mg/kg per hour of propofol via syringe pump. Once the rabbit was anesthetized, a peribulbar injection of 2% lidocaine with hyaluronidase was administered to reduce extraocular muscular movement. The rabbit was securely restrained in a prone position on an adjustable stage for the laser exposure. The rabbit's heart rate and pulse were monitored throughout the experimental protocol, and the rabbit was kept warm by use of warm-water blankets.

Theoretical methods

Nonlinear optical phenomena

Retinal laser lesions for ultrashort (i.e. $\tau < 1$ ns) laser pulses are produced at lower energies than in the nanosecond to microsecond laser pulse regime. During propagation, several nonlinear optical effects may contribute to a change in the characteristics of light impinging the retina and, hence, change the minimum energy required to produce damage. Among these is self-focusing, a phenomenon which can influence the spot size and effective focal length for a given focused beam. Self-focusing can occur in all transparent materials and is a result of the nonlinear refractive index n_2. The total refractive index can be expressed in terms of the linear refractive index n_0, the electric field amplitude squared (i.e., irradiance), and the nonlinear refractive index by: $n = n_0 + n_2 I$. As the peak power increases, the second term in the above equation becomes non-negligible and the refractive index depends, itself, on the electric field strength. For a normal beam with a larger E-field in the center of the beam than at the edges (e.g. gaussian profile), this creates a higher refractive index in the center of the beam than at the edges. Hence, as the beam propagates, there exists a lensing in the area where the beam propagates, and the beam "self-focuses." The result is the ability of the beam to shrink to spot sizes smaller than the diffraction limit for the linear case. In this problem, this translates to smaller retinal image diameters when significant peak powers are contained in the pulse. Above a certain critical threshold, P_{cr}, the beam reaches a point where the cross-section collapses to minimum spot size, and this power is called the critical power for beam collapse.

Marburger [23] numerically determined the critical power for beam collapse to occur when laser peak powers exceed P_2. He found $P_2 = 3.77\,P_1$ where $P_1 = \lambda^2/(8\pi\, n_0 n_2)$ in MKS units. Using these expressions for a 580-nm wavelength and using the measured n_2 for vitreous [26], this analysis predicts critical beam collapse at 1.0 MW of peak power. Below these powers, Marburger found the irradiance was enhanced in the focal plane in a focusing geometry and could be expressed in terms of the peak power in the pulse P, the irradiance without self-focusing I_0, and the second critical power for beam collapse P_2 by:

$$I_{sf} \cong \frac{I_0}{1 - \frac{P}{P_2}}$$

which is valid for $P \leq P_2/4$. Above this limiting power, numerical techniques need to be used to accurately predict the irradiance enhancement.

Soileau et al. [33] verified that Marburger's numerical result [23] is correct for predicting self-focusing effects. Their analysis proves this through extensive experimentation of self-focusing-derived LIB in a focusing geometry. Above P_2 the beam will collapse into a very small filament, and normally other nonlinear optical effects, such as LIB, will be produced due to the high irradiances. At power levels below P_2, there is an enhancement of irradiance due to gradual changes in the spot size with increasing peak power. Using the expression for irradiance enhancement, we find the irradiance can be enhanced by a factor of 33% at the limiting value for validity of the equation ($P = P_2/4$). Above this power, and below the critical power for beam collapse, the irradiance is enhanced, but the equation for I_{sf} underestimates the enhancement factor [33].

Luther et al. [22] estimated the threshold for self-focusing analytically and verified these values numerically. They found that self-focusing initially dominates the dynamics of short-pulse propagation in normally dispersive media, causing an explosive increase in peak intensity resulting in other nonlinear phenomena. They found regimes where self-focusing dominates and regimes where normal group velocity dispersion dominates, as a function of pulsewidth, of spot size, and of wavelength. For powers well above their thresholds, self-focusing dominates, which could result in filamentation and other higher-order processes.

We have previously used the constant shape approximation [27] ($P_{Cr} = P_1$) to determine the role irradiance enhancement might play in changing MVL thresholds. Calculations were made using the diffraction term scaling method of Huang et al. [17]. Soileau et al. [33] determined the irradiance enhancement below beam collapse for I/Io to be as great as twice that expected using the constant shape approximation. They found the irradiance enhancement factor to be 7.15 for $P = 0.9\ P_2$ and 192.00 for $P = 0.99\ P_2$. Our calculations will allow for deviations from the constant shape approximation by adding the factor a to the critical power for beam collapse [31]:

$$P_{cr} = \frac{a\lambda^2}{8\pi n_0 n_2}$$

The factor a was introduced by Sheik-Bahae et al. [31] to account for the deficiencies in the constant shape approximation. This factor is geometry and power dependent and takes values between 3.77 and 6.4. For very large phase distortions and thick samples, as in the current case of the eye, $a = 3.77$, and becomes identical to the results of Marburger [23]. In our calculations we also allow for non-gaussian propagation by including M^2 in the beam propagation. This was done to more closely mimic the characteristics of the eye, which are expected to produce a 10- to 15-μm spot on the retina, where diffraction-limited focusing would produce a 4-μm spot.

LIB model

As a first step in understanding damage caused by LIB in the eye, theoretical models were developed and experimental measurements were made to determine irradiance thresholds corresponding to breakdown in ocular media and in fluids used as simulants for ocular media, such as water and saline solution. An analytic, first-order model [19] was developed to calculate irradiance thresholds for LIB in ocular and aqueous media. The basic assumption underlying the model was that some liquids can be treated as amorphous solids with (effective) conduction and valence bands. This appears to be a reasonable approximation for pure liquid water and for water doped with halide salts [40]. The models of Shen [32], for cascade breakdown in solids, and Keldysh [18], for multiphoton ionization in crystals, have therefore been adapted to model breakdown in aqueous media. Analytic expressions have been obtained for the irradiance thresholds corresponding to multiphoton breakdown, to cascade breakdown, and to initiation of cascade breakdown by multiphoton ionization of seed electrons (multiphoton initiation threshold).

The model includes two different definitions of breakdown, corresponding to two different experimental endpoints. The "flash" endpoint, corresponding to a plasma that emits broadband visible light, has been used in all experimental measurements of LIB thresholds in liquid media for pulsewidths greater than 30 ps. However, for pulsewidths less than 30 ps, another endpoint must be used due to the absence of a broadband visible flash. Zysset et al. [43] used a pump-probe setup to measure the cavitation bubble as the endpoint for breakdown. Hammer et al. [16] used the residual bubble as the endpoint for breakdown. In vivo measurements of the breakdown threshold reported herein and previously [9] likewise used the residual bubble as the endpoint for breakdown. The LIB model calculates the threshold for breakdown based upon critical electron densities of $10^{20}/cm^3$ for the "flash" endpoint and $10^{18}/cm^3$ for the residual "bubble" endpoint. Lower densities are used in the latter case because the creation of a bubble without a broadband visible flash indicates a cooler, less dense plasma. A physical explanation of the breakdown process will make these endpoints more apparent.

When LIB occurs, a plasma is formed. The plasma expands and further ionizes the media and a visible flash is usually emitted from the focal region. The flash is a result of bremsstrahlung emission and electron recombination. The maximum of the broadband spectrum of the flash corresponds to the temperature of the plasma [34]. Hotter plasmas (5000–15000 °K) emit light primarily in the visible region, and cooler plasmas emit light primarily in the infrared. As the plasma expands, a supersonic shock wave and cavitation bubble are created and expand from the focal region. The cavitation bubble can collapse and re-expand a number of times. Upon the final collapse of the cavitation bubble, a residual bubble is created from gas diffusion into the cavity. The residual bubble may remain in the focal volume for a few seconds and is easily observed [12, 39]. Preliminary calculations indicate that the residual bubble cannot be the result of water absorption. Another absorption medium, plasma created by LIB, must be responsible for the residual bubble. Observation of the cavitation bubble threshold via pump-probe experiments [16] has verified this conclusion.

The model has been incorporated into a computer code. The code results have been compared to experimentally measured irradiance thresholds for breakdown of ocular media, saline, and water by nanosecond, picosecond, and femtosecond laser pulses in the visible and near-infrared [20]. The comparison includes data from the literature [10, 11, 29, 38] for infrared nanosecond and picosecond breakdown and from our measurements for visible and infrared pulses ranging in width from 7 ns to 100 fs. In this paper, we compare code results to in vivo rabbit and monkey bubble measurements.

Results

Observations presented herein consist of experimental data and theoretical modeling using input parameters from the experimental setup. These results are presented to provide insight into and explanations for the unexpected phenomena as mentioned in the Introduction. The probit procedure [30] was used to estimate the ED_{50} dose for LIB threshold values for breakdown and bubble generation. Enough data points were obtained to ensure that the fiducial limits were reasonably narrow.

Experimental results

In vivo minimum visible lesion thresholds were measured in the rhesus monkey eyes [8] and are presented in Fig. 2 for five pulsewidths between 4 ns and 90 fs. The values shown in the graph are for single pulse energies calculated with probit analysis (ED_{50} values) and were obtained at the 24-h reading of the lesions. As can be seen in the figure, all threshold values are below 1 μJ. The slopes [8] of the probit curves were calculated between the ED_{85} and the ED_{50} values and are presented in Fig. 3 as a bar graph for the five fixed values of pulsewidth. This graph shows that all slopes are greater than 2, with the exception of that at 90 fs, which is 1.58. The value at 600 fs is 4.11, which also happens to occur with the lowest energy threshold (0.26 μJ).

The in vivo threshold for LIB (i.e., bubble generation for 120-fs, 580-nm pulses) within the rhesus monkey eye was measured within a single eye but at a different site for each exposure. A probit analysis was performed on 66 data points, and an ED_{50}value of 0.56 μJ was calculated, along with fiducial limits of 0.46 and 0.69 μJ. Other points of interest are the ED_{10} and ED_{90}, which were 0.32 (0.19–0.40) μJ and 1.0 (0.79–1.6) μJ, respectively. As expected, all pulses with energies of 1.5 μJ and greater (60 shots) produced a bubble within the vitreous of the eye. LIB threshold measurements previously reported [4, 9, 16] are included in Table 1 along with the present results for a new artificial eye and for the monkey eye.

The LIB threshold measured for the artificial eye was determined to be 0.27 (0.26–0.28) μJ for a measured image diameter of 5.7 ± 0.7 μm using nanojoule pulses. As with the other measurements, these were for the bubble threshold as observed on a video camera, magnified with a long working distance microscope objective. Also listed in this table are previously reported thresholds and other pertinent data for each measurement, such as estimated and/or measured diameters in micrometers of the focused laser beam and the calculated peak powers of the LIB thresholds.

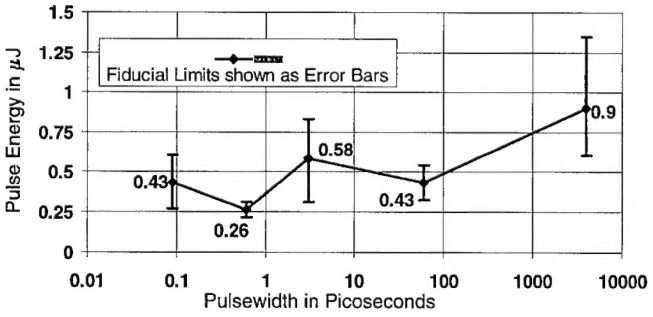

Fig. 2 In vivo MVL-ED_{50} thresholds vs pulsewidth

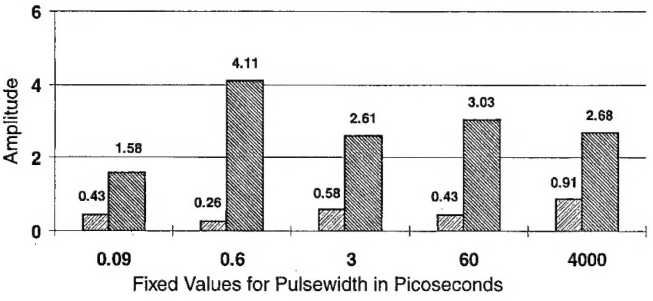

Fig. 3 Slopes of probit curves and MVL thresholds

Theoretical modeling results

Self-focusing model

We calculated the changes that occur to the retinal spot size. These calculations did not include linear dispersion and other effects important for very short femtosecond laser pulses (less than 300 fs). Figure 4 shows the calculated spot size at the retina as a function of incident peak power. Included are the effects of non-gaussian propaga-

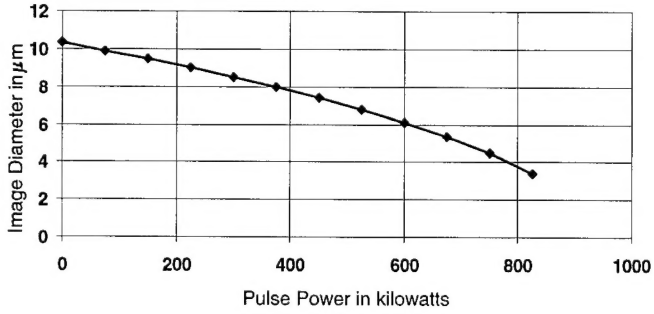

Fig. 4 Graph of the retinal spot size vs.the peak power in the laser pulse at a wavelength of 580 nm

Table 1 Laser-induced breakdown (*LIB*) threshold energies and peak powers in laser beam

	H_2O Hammer [16]	H_2O Boppart [4]	H_2O eye, artificial	Albino rabbit eye, in vivo [9]	Rhesus monkey eye, in vivo
LIB energy (μJ)	1.3	1.5	0.27	9.5	0.56
Retinal image (μm)	17	20	5.7	30	10
Pulsewidth (fs)	120	100	150	120	120
Peak power (MW)	10.8	12.5	1.9	77	4.6

tion ($M^2 = 4$) and corrections to the constant shape approximation. As shown, the spot size can decrease by a factor of 3, and therefore the irradiance is expected to be enhanced by a factor of 10 or more. For tightly focusing geometries such as the eye, the LIB threshold can be below the critical power for beam collapse [33]. For these calculations, the nonlinear refractive indices of vitreous and aqueous humor were taken from measurements [26] made at 60 ps.

LIB model

Our LIB model was used to calculate the breakdown threshold irradiances (bubble formation thresholds) in pure water as a function of pulsewidth between 50 fs and 3 ps. A wavelength of 580 nm and a focal diameter of 10 μm were used for all calculations. It was not necessary to calculate the thresholds beyond 3 ps since we are interested in very small energies, and we have determined that for longer pulsewidths, these small energies are not likely to cause breakdown. Figure 5 is a graph of irradiance thresholds calculated versus pulsewidth for both multiphoton breakdown and cascade breakdown. The model and the graph clearly show that breakdown changes from a cascade to a multiphoton process as the pulsewidth decreases to the low femtosecond regime. The crossover point occurs at approximately 165 fs, as indicated on the graph.

In Fig. 6, we present the breakdown thresholds in terms of pulse energy as a function of pulsewidth for a laser beam focused to a 10-μm image diameter at the retina and at the lower of the two irradiance thresholds from Fig. 5. The irradiances were converted to pulse energies by using the areas of the retinal images. A line was drawn through the points as an aid to the eye only.

Figure 7 shows a different set of calculations in which we present the breakdown pulse energy versus the retinal image diameter for a 100-fs pulse. For 100-fs pulses, breakdown is by multiphoton ionization only and occurs at a constant irradiance threshold of 5.4×10^{12} W/cm^2 regardless of focal spot size. The energy threshold is thus proportional to focal area. As shown, the pulse energy drops from 42 μJ at an image diameter of 100 μm to only 0.1 μJ at a 5-μm image diameter. Coincidentally, the LIB threshold at 100 fs for a retinal image diameter of 10 μm is only 0.43 μJ, the exact value which was found for the MVL- ED_{50} threshold at 90 fs.

Another set of data was calculated to show the irradiance versus the distance from the retina (fundus) in micrometers for a 50-μJ, 100-fs pulse. An input beam of 2.5 mm diameter at the cornea is focused to a 10-μm image at the retina (Fig. 8). This pulse energy was used because it is a little over 100 times the MVL-ED_{50}

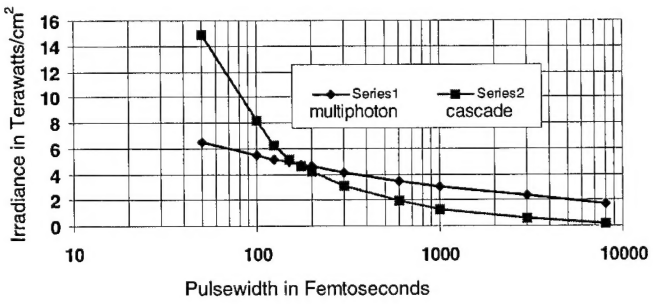

Fig. 5 Model LIB threshold irradiance vs pulsewidth

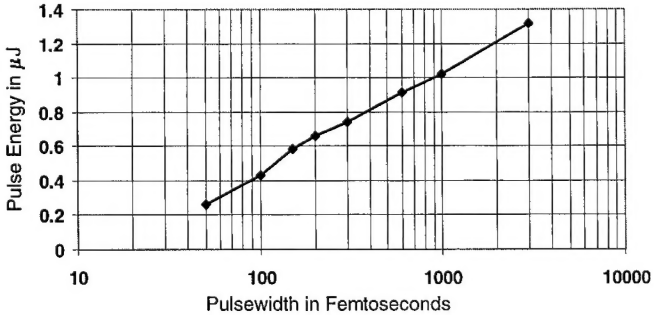

Fig. 6 Model LIB threshold energy vs pulsewidth for an image diameter of 10 μm

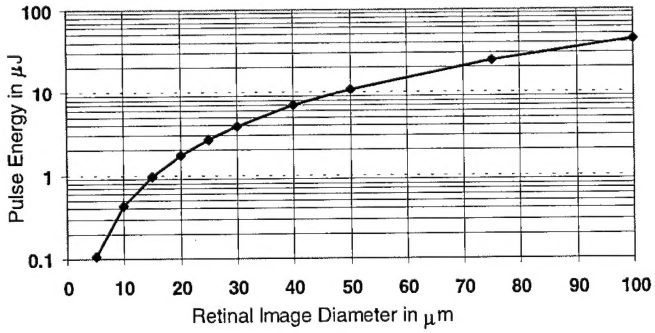

Fig. 7 Model LIB threshold energy vs retinal image diameter for a 100-fs pulse

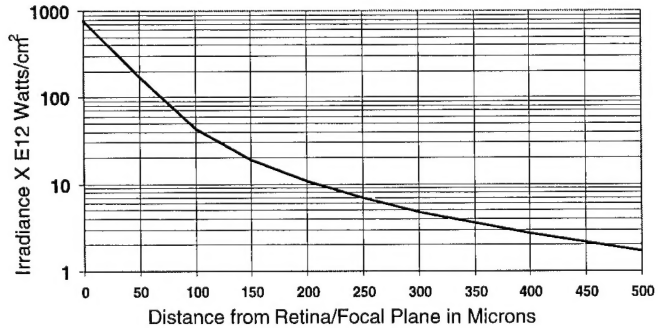

Fig. 8 Irradiance vs distance from retina for a 50-μJ, 100-fs pulse

threshold for the monkey eye of 0.43 μJ. Retinal damage by pulses of 100 times the MVL-ED_{50} energy has been studied by other researchers [2, 42] and by our group [8]. These results show that damage to the retina does not scale linearly with energy. It can be seen in Fig. 8 that the water LIB threshold value of 5.4×10^{12} W/cm^2 occurs at a distance of 280 μm anterior to the retina when the eye focuses the retinal image to a 10-μm diameter. Another way to explain it is that, at the retina, for a 10-μm image diameter, the irradiance within the laser pulse would be 740×10^{12} W/cm^2, or 137 times the LIB threshold value. Also, it should be pointed out that these values occur without any self-focusing. Self-focusing would extend the point at which the LIB threshold is reached to more than 280 μm from the retina.

Discussion

The in vivo MVL-ED_{50} thresholds for visible wavelengths in the rhesus monkey eye show a declining trend with pulsewidth. All thresholds measured in this study are lower than any other thresholds reported in the literature, with the exception of the single data point at 6 ps (530 nm) for the monkey eye [5], which was 0.24 μJ. At 4 ns (532 nm), our MVL-ED_{50} threshold was measured to be 0.90 μJ, which is less than an order of magnitude above the maximum permissible exposure (MPE) as defined by the ANSI-Z136.1 standard [1]. At 60 ps (532 nm), our threshold was 40 times less than the value (18 μJ) reported by Goldman et al. [14] at 30 ps and 532 nm. Our value at 3 ps (580 nm) is more than twice as large as Bruckner and Taboada's [5] value at 6 ps and 530 nm (0.58 vs 0.24 μJ); however, this difference could be partially accounted for by the difference in wavelength. For all three probit curves representing nanosecond and picosecond pulse damage, the slopes were larger than 2, which provides some indication that the data range between no lesions and all lesions was relatively narrow and that only one damage mechanism may be operating.

As the pulsewidth was reduced to the femtosecond range, the threshold decreased and the data at 600 fs (580 nm) had the lowest threshold (0.26 μJ) and the greatest slope (4.1). As the pulsewidth was further reduced to 90 fs, the ED_{50} became larger (0.43 μJ), and the slope of the probit curve was below 2 (1.58). This low value of slope was caused by the slow transition between no lesions at low-energy pulses and all lesions at the higher-energy pulses. This transition occurred between 0.1 and 1.4 μJ (i.e., 0.1 μJ sometimes produced a visible lesion and 1.4 μJ did not always produce a lesion). This low slope, coupled with damage data for suprathreshold laser pulses at 90 fs (damage not proportional to pulse energies), indicated a possible difference between damage mechanisms at 600 fs and 90 fs. Both Birngruber et al. [2] and Zuclich et al. [42] reported failure to create hemorrhages in the rabbit fundus at 100 times threshold energies and also that the damage was not proportional to pulse energy. We performed theoretical modeling coupled with experimental data to try to understand the mechanisms which produce these unexpected results.

We first looked at self-focusing effects [7, 9, 27] and possible beam collapse [22] to ascertain whether they could be influencing our data and to determine the range of parameters over which they occur. In order to determine whether self-focusing of the laser pulse occurs in the eye, the nonlinear index of refraction, n_2, must be known for the components of the eye. This nonlinear index of refraction was measured in both human and rabbit vitreous, in water, and in saline, and compared [26] with the previously measured value for water. A model was then developed to utilize this index in the propagation of the laser pulse to the fundus as a function of the peak power within the pulse. Figure 4 shows how the retinal image diameter should decrease due to self-focusing as a function of laser beam peak power for hundreds of kilowatts of peak power. This analysis will change for pulses in the low femtosecond regime when other propagation effects may occur.

A search of the literature revealed the results shown in Table 2, which lists the wavelengths, pulsewidths, and energies reported for MVL thresholds. Also included are the species of animal used and the peak power in kilowatts, calculated from the energy and pulsewidth. Figure 9 graphically illustrates the peak pulse power as a function of pulsewidth used in only monkey MVL-ED_{50} studies. There is a near-linear trend seen in the data from the microsecond to femtosecond regime. This trend is shown pictorially by the solid line, which is just a guide to the eye. As can be seen in Table 2 and Fig. 9, only four MVL thresholds (one for monkey data) had peak powers

Table 2 Peak power reported for visible thresholds

Researchers	Wavelength (nm)	Pulse-width	Energy (μJ)	Peak power (kW)
Bruckner et al. [5] Monkey	530	6 ps	0.24	40
Taboada et al. [35] Monkey	1060	6 ps	2.2	370
Goldman et al. [14]	532	30 ps	18	600
Monkey	1064	30 ps	8.7	290
Ham et al. [15] Monkey	1064	30 ps	12.9	430
Birngruber et al. [2] Rabbit	625	80 fs	4.5	56000
Zuclich et al. [42]	580	5 ps	2.6	520
Rabbit	580	500 fs	1.1	2200
	580	90 fs	1.1	12200
Cain et al. [8]	580	3 ps	0.58	193
Monkey	580	600 fs	0.26	430
	580	90 fs	0.43	4800

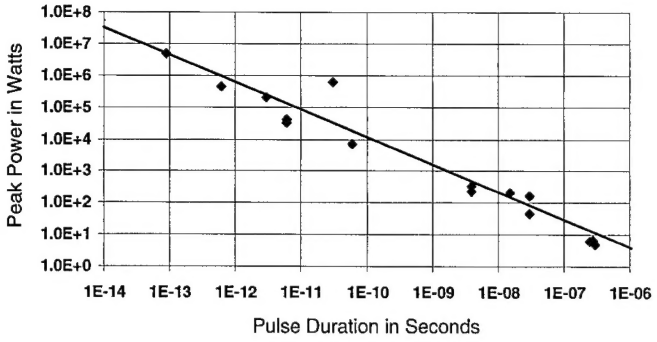

Fig. 9 Visible wavelength MVL data available for rhesus monkey eyes, plotted as peak pulse power vs pulse duration

greater than 1 MW which could possibly be high enough to cause critical beam collapse. Using the expression for irradiance enhancement, we find the irradiance can be enhanced by a factor of 50% at the limiting value for validity of the equation $P = P_2/4$. Above this power and below the critical power for beam collapse, the irradiance is enhanced, but the equation for I_{sf} underestimates the enhancement factor. For tightly focusing geometries such as the eye [27], the LIB threshold can be below the critical power for beam collapse. From Figs. 4 and 9, we can determine that self-focusing will have an appreciable effect on the retinal fluence for pulse durations less than 1 ps. At some pulsewidths, we expect the LIB threshold to be lower than the critical beam collapse threshold, and a new phenomena may be responsible for retinal damage.

In this paper we suggest that self-focusing did occur within our 90-fs pulse MVL measurements and that at 600 fs it may have acted to only reduce the retinal image diameter, thereby increasing the retinal irradiance and minimizing the amount of energy needed to cause visible damage. Our results indicate that self-focusing may have occurred, but not beam collapse, with these pulses. In cases where the beam did collapse, some other nonlinear phenomenon could have occurred, such as LIB. We know that LIB does absorb some of the energy of the pulse as well as provide some shielding to the retina [4].

Figure 5 shows the results of our LIB model calculations as a function of pulsewidth for water and includes thresholds for both multiphoton and cascade breakdown. It can be seen that cascade breakdown is clearly the dominant mechanism for pulsewidths greater than 300 fs and, as the pulsewidth is reduced, the breakdown mechanism switches from cascade to multiphoton ionization. For pulsewidths below 165 fs, multiphoton breakdown has a lower threshold, and the multiphoton threshold changes slowly with pulsewidth while cascade thresholds increase exponentially as the pulsewidth decreases. Figure 6 is a plot of the lower threshold irradiances of Fig. 5 converted to pulse energy by using the pulsewidths and a retinal image diameter of 10 μm. These LIB threshold energies are plotted as a function of the pulsewidth for pulses down to 50 fs. Although the threshold irradiances increase by more than an order of magnitude as the pulsewidth is decreased from 3 ps to 50 fs, the pulse energy actually decreases by a factor of 5. If we compare our MVL-ED_{50} thresholds with the LIB thresholds shown in Fig. 6, it can been seen that the 0.58 μJ at 3 ps and the 0.26 μJ at 600 fs are both very much below the threshold curve. Thus, it is highly unlikely that LIB would contribute to MVL creation for these pulsewidths. However, if we consider the 90-fs MVL-ED_{50} threshold of 0.43 μJ and compare it to the 0.40-μJ (90 fs) LIB threshold shown in Fig. 6, it is possible that LIB will occur in the fundus or vitreous with these pulse energies if the retinal image size is close to 10 μm in diameter. This shows that LIB could occur in the vitreous even without self-focusing.

In all of our MVL measurements, we did not attempt to observe or record any LIB or bubble generation at any pulsewidth. Therefore breakdown could have been occurring, especially at the 90-fs pulsewidths, and we would not have known, because no permanent damage has ever been directly connected to LIB. However, when we monitored the retina and fundus with a modified fundus camera (see Fig. 1) and a color video camera during and after the exposures, we were able to observe the bubbles being generated. Bubbles were observed with pulse energies as low as 0.31 μJ in the monkey eye, and the LIB-ED_{50} threshold was determined to be 0.56 (0.46–0.69) μJ. Thus we not only know that bubbles are generated at pulse energies around 0.5 μJ at 100 fs; but for pulse energies below 0.3 μJ, no bubbles were observed, and for pulse energies above 1.5 μJ every pulse (60 shots) produced a bubble.

When we consider the curve shown in Fig. 7 for a fixed pulsewidth of 100 fs and a range of retinal image diameters between 5 and 15 μm, we find that the LIB threshold pulse energies change by an order of magnitude, from 0.1 μJ to 1.0 μJ. This large change is due to the irradiance being a function of retinal image area, which changes as a squared function of image diameter. The LIB threshold measured for the artificial eye was found to be 0.27 μJ. The image diameter measured in the artificial eye with nanojoule pulses was found to be 5.7 ± 0.7 μm. We estimated the retinal image size in the rhesus monkey to be 10 μm from our measurements and other reported estimates for the monkey eye. This estimate does not assume any self-focusing effects from the high peak powers, and, if it did, the spot size could be much less than 10 μm. Thus, both LIB threshold values, for artificial and monkey eye, were found to be within the model-calculated thresholds for image diameters between 5 and 15 μm.

The data in Fig. 8 were calculated using a suprathreshold pulse energy of 50 μJ to show that the LIB threshold of 5.4 tW/cm^2 for a 100-fs pulsewidth can be obtained at distances far from the retina. This is due to

the simple focusing of the pulse by the optics of the eye with no self-focusing. This graph shows that a 2.5-mm diameter laser beam into the eye produces a 10-μm diameter image at the retina and the irradiance becomes 740 tW/cm^2, or 137 times the LIB threshold value. In fact, for distances out to 280 μm from the retina, the irradiances in the vitreous are still above threshold values. We have observed and recorded this breakdown phenomena on video within the artificial eye, with the breakdown occurring up to 300 μm in front of the focal point for 100 times threshold pulse energies. In this case, the bubble extends from the focal point throughout the 300 μm in the shape of a cone. These data show that LIB can occur within the vitreous for suprathreshold pulses and may even produce multiple breakdown points before reaching the retina.

In conclusion, we have discussed the roles that self-focusing and LIB can potentially play when visible, ultrashort laser pulses propagate from the cornea to the retina. Such nonlinear mechanisms assist our understanding of the anomalies observed in the MVL data. We have shown that self-focusing is predicted to occur when the laser beam peak powers approach megawatt levels, as they routinely do with the shorter (i.e., less than 10 ps) pulsewidths. Our studies, coupled with others, indicate that femtosecond pulses propagating from the cornea to the retina might undergo self-focusing and/or beam collapse. This would reduce the retina spot size, thus increasing the retinal irradiance and increasing the probability of LIB at or near the retina. Even if LIB did not occur, increased retinal focusing would lower the corneal fluence required for damage.

We have shown, with an analytical model coupled to experimental data, that LIB and bubble generation can and do occur within monkey eyes at pulse energies below 1 μJ. A bubble generation threshold of 0.56 μJ, with fiducial limits of 0.46 and 0.69 μJ, was measured for 120-fs pulses in the rhesus eye. Even the higher fiducial limit is within 0.25 μJ of the rhesus MVL-ED_{50} threshold (0.43 μJ) measured for 90-fs pulses. This suggests that LIB might influence MVL threshold measurements for pulses in the femtosecond regime. For example, shielding effects of LIB and bubble formation may explain why the probit slope for 90-fs MVL data is below 2. It may also explain why femtosecond pulses with energies 100 times the MVL threshold level do not always cause hemorrhagic lesions and/or damage to the retina proportional to that which occurs with longer pulses. In conclusion, nonlinear effects must be considered and examined thoroughly for visible femtosecond laser pulses, even at pulse energies below 1 μJ.

Acknowledgements The research reported here was performed at the Optical Radiation Division, Armstrong Laboratory, Brooks AFB, Texas, and was supported by the Air Force Office of Scientific Research (grant 2312AA-92AL014) and the USAF Armstrong Laboratory (contract F33615-92-C-0017).

References

1. ANSI (1993) American national standard for the safe use of lasers. American National Standards Institute, Inc., New York
2. Birngruber R, Puliafito CA, Gawande A, Lin W, Schoenkin R, Fujimoto JG (1987) Femtosecond laser-tissue interactions: retinal injury studies. IEEE J Quant Electron 23:1836–1844
3. Blankenstein MF, Zuclich JA, Allen RG, Davis H, Thomas SJ, Harrison R (1986) Retinal hemorrhage thresholds for Q-switched neodymium-YAG laser exposures. Invest Ophthalmol Vis Sci 27:1176
4. Boppart SA, Toth CA, Roach WP, Rockwell BA (1993) Shielding effectiveness of femtosecond laser-induced plasmas in ultrapure water. SPIE 1882:347
5. Bruckner AP, Taboada J (1982) Retinal tissue damage induced by 6 psec 530-nm laser light pulses. Appl Opt 21:365–367
6. Bruckner AP, Schurr JM, Chang EL (1980) Biological damage threshold induced by ultrashort 2nd and 4th harmonic light pulses from a mode-locked Nd:glass laser. SAM-TR-80–47
7. Cain CP, Toth CA, Stein CD, Noojin GD, Stolarski DJ, Rockwell BA, Boppart SA, Roach WP (1994) Femtosecond laser threshold: Retinal damage versus induced breakdown mechanisms. SPIE 2134A:22–27
8. Cain CP, Toth CA, DiCarlo CD, Stein CD, Noojin GD, Stolarski DJ, Roach WP (1995) Visible retinal lesions from ultrashort laser pulses in the primate eye. Invest Ophthalmol Vis Sci 36:879–888
9. Cain CP, DiCarlo CD, Noojin GD, Amnotte RE, Roach WP (1995) In vivo laser-induced breakdown in the rabbit eye. SPIE 2391:41–47
10. Docchio F, Dossi L, Sacchi CA (1986) Q-switched Nd:YAG laser irradiation of the eye and related phenomena: an experimental study. I. Optical breakdown determination for liquids and membranes. Lasers Life Sciences 1:87–103
11. Docchio F, Sacchi CA, Marshall J (1986) Experimental investigation of optical breakdown thresholds in ocular media under single pulse irradiation with different pulse durations. Lasers Ophthalmol 1:83–93
12. Felix MP, Ellis AT (1971) Laser-induced liquid breakdown – a step-by-step account. Appl Phys Lett 19:484–486
13. Goldman AJ, Ham WT, Mueller HA (1975) Mechanisms of retinal damage resulting from the exposure of rhesus monkeys to ultrashort laser pulses. Exp Eye Res 21:457–469
14. Goldman AJ, Ham WT, Mueller HA (1977) Ocular damage thresholds and mechanisms for ultrashort pulses of both visible and infrared laser radiation in the rhesus monkey. Exp Eye Res 24:45–56
15. Ham WT, Mueller HA, Goldman AJ, Newman BE, Holland LM, Kuwabara T (1974) Ocular hazard from picosecond pulses of Nd:YAG laser radiation. Science 185:362–363
16. Hammer DX, Thomas RJ, Noojin GD, Rockwell BA (1995) Ultrashort pulse laser induced bubble creation thresholds in ocular media. SPIE 2391:30–40
17. Huang D, Ulman M, Acioli LH, Haus HA, Fujimoto JG (1992) Self-focusing-induced saturable loss for laser mode locking. Opt Lett 17:511–513

18. Keldysh LV (1965) Ionization in the field of a strong electromagnetic wave. Phys JETP 20: 1307–1314
19. Kennedy PK (1995) A first-order model for computation of laser-induced breakdown thresholds in ocular and aqueous media. I. Theory. IEEE J Quant Electron 31: 2241–2249
20. Kennedy PK, Boppart SA, Hammer DX, Rockwell BA, Noojin GD, Roach WP (1995) A first-order model for computation of laser-induced breakdown thresholds in ocular and aqueous media. II. Comparison to experiment. IEEE J Quant Electron 31: 2250–2257
21. Lund DJ, Beatrice ES (1989) Near infrared laser ocular bioeffects. Health Phys 56: 631–636
22. Luther GG, Moloney JV, Newell AC (1994) Self-focusing threshold in normally dispersive media. Opt Lett 19: 862–864
23. Marburger JH (1975) Self-focusing theory. Prog Quant Electron 4: 86
24. Roach WP, Cain CP, Toth CA, Stein CD (1991) Ocular effects of ultrashort pulsewidth laser radiation. USAFSAM Protocol RZV-91–04
25. Roach WP, Toth CA, Stein CD, Noojin GD, Stolarski DJ, Cain CP (1994) Minimum visible lesions from pico- and femtosecond laser pulses. SPIE 2134A: 10–21
26. Rockwell BA, Roach WP, Rogers ME, Mayo MW, Toth CA, Cain CP, Noojin GD (1993) Nonlinear refraction in vitreous humor. Opt Lett 18: 1792–1794
27. Rockwell BA, Roach WP, Rogers ME (1994) Determination of self-focusing effects for light propagating in the eye. SPIE 2134A: 2–9
28. Rockwell BA, Kennedy PK, Thomas RJ, Roach WP, Rogers ME (1995) The effect of nonlinear optical phenomena on retinal damage. SPIE 2391: 89–95
29. Sacchi CA (1991) Laser-induced electric breakdown in water. J Opt Soc Am B 8: 337–345
30. SAS Institute (1994) SAS probit procedure. Cary, NC
31. Sheik-Bahae M, Said AA, Hagan DJ, Soileau MJ, Van Stryland EW (1991) Nonlinear refraction and optical limiting in thick media. Opt Eng 30: 1228
32. Shen YR (1984) The principles of nonlinear optics. Wiley, New York
33. Soileau MJ, Williams WF, Mansour N, Van Stryland EW (1989) Laser-induced damage and the role of self-focusing. Opt Eng 28: 1133–1144
34. Stolarski DJ, Hardman J, Bramlette CM, Noojin GD, Thomas RJ, Rockwell BA, Roach WP (1995) Integrated light spectroscopy of laser-induced breakdown in various aqueous media. SPIE 2391: 100–109
35. Taboada J, Gibbons WD (1978) Retinal tissue damage induced by single ultrashort 1060 nm pulses. Appl Opt 17: 2871–2873
36. Toth CA, Cain CP, Roach WP, Stein CD, Allen RG, Elliott WR, Zuclich JA (1993) Retinal effects of ultrashort laser pulses. Invest Ophthalmol Vis Sci 34: 960
37. Toth CA, Cain CP, Stein CD, Noojin G, Stolarski D, Zuclich JA, Roach WP (1995) Retinal effects of ultrashort laser pulses in the rabbit eye. Invest Ophthalmol Vis Sci 36: 1910–1917
38. Vogel A, Busch S, Jungnickel K, Birngruber R (1994) Mechanisms of intraocular photodisruption with picosecond and nanosecond laser pulses. Lasers Surg Med 15: 32–43
39. Vogel A, Schweiger, P, Priser A, Asiyo MN, Birngruber R (1990) Intraocular Nd:YAG laser surgery: Light-tissue interactions, damage range, and reduction of collateral effects. IEEE J Quant Electron 26: 2240–2259
40. Williams F, Varma SP, Hillenius S (1976) Liquid water as a lone-pair amorphous semiconductor. J Chem Phys 64: 1549–1554
41. Zuclich JA, Elliott WR, Coffey DJ (1992) Suprathreshold retinal lesions induced by laser radiation. Lasers Light Ophthalmol 5: 51–59
42. Zuclich JA, Elliott WR, Cain CP, Noojin GD, Roach WP, Rockwell BA, Toth CA (1993) Ocular damage induced by ultrashort laser pulses. AL-TR-93–0099
43. Zysset B, Fujimoto JG, Deutsch TF (1989) Time-resolved measurements of picosecond optical breakdown. Appl Phys B 48: 139–147

Graefe's Arch Clin Exp Ophthalmol (1996)
234: S 38–S 41

Benedetto Ricci
Alessandro Santo
Francesco Ricci
Giuseppe Minicucci
Fernando Molle

Scleral buckling surgery in stage 4 retinopathy of prematurity

Received: 28 March 1995
Revised version received:
27 September 1995
Accepted: 9 October 1995

B. Ricci (✉) · A. Santo
Department of Ophthalmology,
Policlinico Universitario, Via Consolare
Valeria, I-98123 Messina, Italy,
Fax +39-90-2924819

F. Ricci · G. Minicucci · F. Molle
Department of Ophthalmology,
Catholic University of Rome, Italy

Abstract ● Background: Technical advances in neonatal intensive care have significantly increased the number of very low birth-weight babies that survive the perinatal period. Some of these infants develop severe retinopathy of prematurity that may lead to retinal detachment. ● Methods: Between November 1988 and January 1994, 28 eyes from 15 preterm babies underwent scleral buckling for stage 4 retinopathy of prematurity at a mean age of 4.2 months. Cryotherapy was performed preoperatively on 12 eyes and intraoperatively in the remaining 16 eyes. The mean follow-up period was 35 months. ● Results: Scleral buckling produced retinal reattachment in 13 eyes (46.4%). Severe myopia (−5 D to −15 D) was found in all 13 of these eyes; 12 also presented convergent strabismus. Mean visual acuity, measured in 6 eyes from children over the age of 3 years was 20/40. In 7/28 eyes of the younger children of this group we found a fix and follow the light capability. No light perception was detected in 11/28 eyes; in the remaining 4/28 eyes there was only light perception. Scleral buckling failed to prevent the progression to stage 5 in 15 eyes (53.6%). Additional surgery was excluded for 9 of these eyes based on ultrasonography findings; the other 6 eyes underwent vitrectomy, which led to macular reattachment in 4 cases. ● Conclusions: Clinical experience shows that scleral buckling is not always capable of preventing progression of the disease to stage 5. Furthermore, even when the anatomic results of this procedure are good, the functional outcome is often complicated by severe visual impairment.

Introduction

Technical advances in neonatal intensive care have significantly increased the number of very low birth-weight infants that survive the perinatal period. The incidence of retinopathy of prematurity (ROP) among these preterm infants varies from 60% to 80% [2, 4]. Although spontaneous regression of the disease occurs in the majority of these cases, the results of the Cryo-ROP Study [2] indicate that 7.5% of cases will progress to a disease stage requiring cryotherapy, and one fourth of all treated cases will subsequently develop retinal detachment. This phase of ROP is described as stage 4A or 4B, depending on whether or not the detachment involves the macula [1]. One of the most commonly used surgical approaches for treatment of stage 4 ROP is scleral buckling. According to Trese [11], the objective of this type of surgery is reattachment of the retina and prevention of progression to stage 5. The present study represents a retrospective analysis of the results of scleral buckling in 28 eyes from 15 infants with stage 4A or 4B ROP.